PULSED FIELD LIMITS IN SRF CAVITIES*

J. T. Maniscalco†, D. Gonnella, D. L. Hall, P. N. Koufalis, and M. Liepe

CLASSE, Cornell University, Ithaca, NY, 14853, USA

Abstract

High-power pulsed (HPP) measurements of SRF cavities offer several different avenues of experimentation from standard continuous wave (CW) measurements by probing higher fields and reducing thermal effects. In this paper we report upon recent measurements of N-doped Nb and Nb_3Sn cavities, investigating the limitations of the superheating field, flux entry field, and other maximum fields. We also investigate the potential of these materials for operation in a pulsed accelerator, which would partially or fully mitigate the effects of defects (i.e. thermal quenches).

INTRODUCTION

A major figure of merit for superconducting radio-frequency (SRF) cavities is the quench field, the highest magnetic field achievable on the RF surface before causing a transition to the normal-conducting state. This transition can be caused by a number of factors, including flux entry, field enhancement at surface defects, thermal runaway, and ultimately the superheating field. For continuous-wave (CW) accelerators, thermal runaway is a significant limitation. However, for pulsed accelerators, one can adjust the pulse width and pulse frequency to allow the cavity to return to thermal equilibrium between pulses, thus mitigating the effect of thermal runaway and allowing the cavity to reach higher peak fields.

METHODS

Pulsed testing provides insights into this changing quench field [1]. By avoiding the limitation of thermal equilibrium, it is possible to probe other limiting factors. In particular, one can determine whether a cavity is limited by localized flux entry or localized defect heating or if it is limited globally by reaching a critical field. To make this distinction, we analyze the peak surface field during a quenching pulse as a function of the temperature of the cavity. Typically, critical field limitations approximately follow the relation given in Eq. (1), where H_{pk} is the peak surface field reached during the pulse, T is the experimental temperature, T_c is the critical temperature of the superconductor, and H_{crit} is a critical field, such as the superheating field H_{sh}, measured at $T = 0$.

$$H_{pk} = H_{crit}\left[1 - \left(\frac{T}{T_c}\right)^2\right] \quad (1)$$

On the other hand, flux entry and defect heating limitations follow a relation with temperature that approaches the low-temperature quench field asymptotically as temperature decreases. At high temperatures, cavities with these limits tend to revert to the limit of H_{sh}, which is much lower at high temperature than at low temperature.

We present here results from three cavities. The first cavity, here labeled LTE1-2, was doped with nitrogen according to the following protocol: the cavity underwent a 900 °C bake for 20 minutes in a 60 mTorr N_2 environment, followed by a 30 minute anneal, with a final removal of 18 µm by vertical electropolishing (VEP). The second cavity, LTE1-3, was also doped with nitrogen, but with a 990 °C bake for 5 minutes in 20 mTorr of N_2, with no annealing phase, and with 5 µm of VEP removal. The final cavity, LTE1-6, was coated with niobium-3-tin (Nb_3Sn) with a 24-hour degas, 5 hours of nucleation at 500 °C, 3 hours of coating at 1100 °C, and finally a 6 hour annealing phase at 1100 °C [2, 3].

Testing was performed using a 1 MW Klystron with 100 µs pulses, at a rate of ~1 Hz. Cavities were mounted in a vertical test dewar.

RESULTS AND ANALYSIS

Nitrogen-Doped Cavities

Figure 1 shows the measurements of peak surface magnetic field achieved in cavity LTE1-2 as a function of temperature. At high temperature, the peak field very closely followed the superheating field, calculated from material parameters using Ginzburg-Landau (GL) theory, and following the temperature dependence of Eq. (1) with $B_{sh} = \mu_0 H_{sh} = 186$ mT. At lower temperature, the quench field quickly leveled off, approaching 100 mT at low temperatures. This was above both the CW quench field of 64 mT at 2.0 K and the estimated lower critical field $B_{c1} = 37$ mT. This performance was consistent with a defect limitation, either by a normal conducting region or by flux entry above H_{c1}.

Figure 2 shows the relation between time to quench and peak field at the quench. The time to quench was measured as the time difference between the start of an RF pulse and the time that the cavity quenched. The behavior of the cavity very closely follows the thermal model: with fixed temperature, the power of the pulses was adjusted to change the filling speed of the cavity, thereby adjusting the filling time. For longer filling times, i.e. longer time to quench, thermal runaway effects had a stronger presence; as a result, though the time to reach quench was longer, the peak field at time of quench was lower. Again, these quenches occurred at significantly higher fields than the CW quench field, and indeed, at longer times to quench, the peak field asymptotically

* This work supported by NSF award PHY-1416318 and DOE award DE-SC0008431.

† jtm288@cornell.edu

ISBN 978-3-95450-147-2

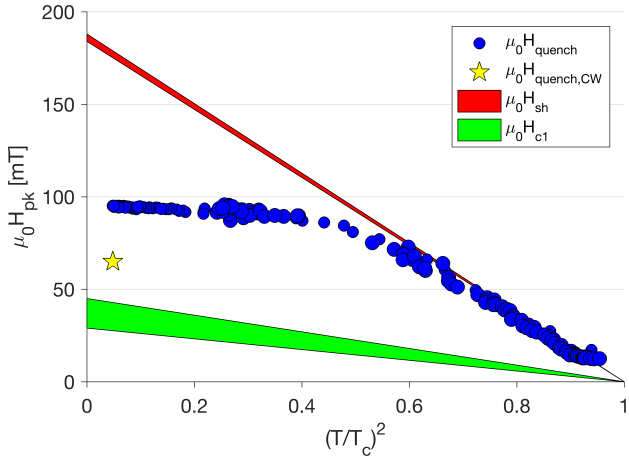

Figure 1: Peak surface magnetic field as a function of temperature for cavity LTE1-2 at 1 MW of Klystron power, shown here on the scale of $(T/T_c)^2$. At high temperatures, the peak field matches the superheating field calculated from GL theory for the mean free path of the RF penetration layer; at low temperatures, the peak field asymptotically approaches a maximum. All quenches happened above H_{c1}, the lower critical field.

approached the CW quench field. This is consistent with a defect limitation, with either a normal-conducting region appearing or with localized flux entry at a defect location.

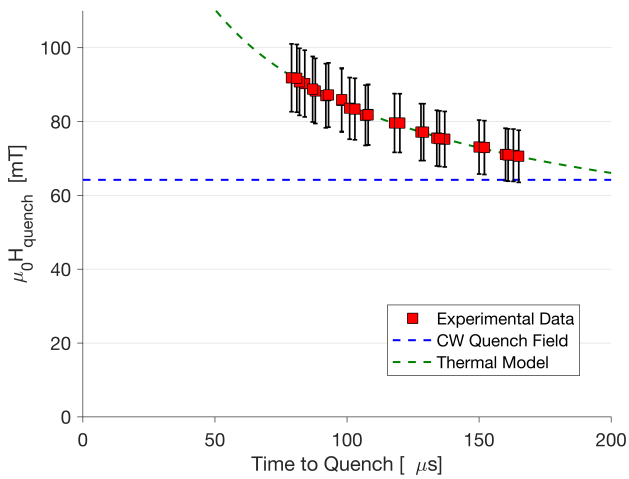

Figure 2: Pulsed quench field is shown here as a function of time to reach quench for cavity LTE1-2. Here, longer times at lower quench field indicate a thermal effect, consistent with a defect limitation.

Figures 3 and 4 show the peak surface magnetic field vs. temperature and vs. time to quench, respectively, for the second N-doped cavity, LTE1-3. LTE1-3 exhibited very similar performance to LTE1-2, again consistent with the thermal model of a defect limitation. For this cavity, B_{c1} is estimated from material parameters to be 26 mT, the CW quench field was 40 mT, the peak low-temperature pulsed quench field was 70 mT, and the superheating field B_{sh} was estimated to be 179 mT.

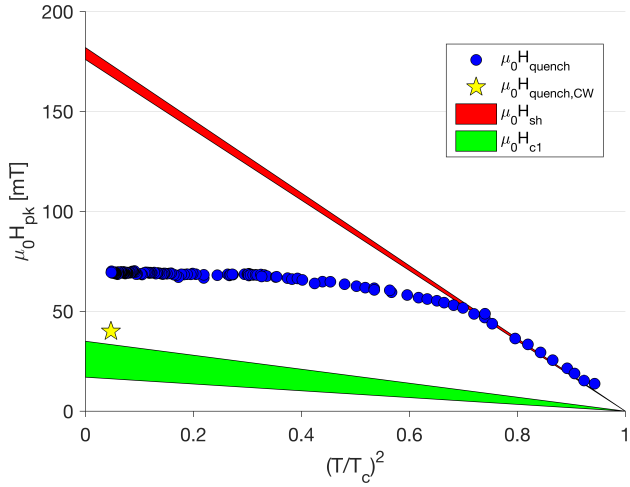

Figure 3: Peak surface magnetic field as a function of temperature for cavity LTE1-3, shown here on the scale of $(T/T_c)^2$. Performance here was qualitatively very similar to LTE1-2, though both the CW quench field and low-temperature pulsed quench field were lower here.

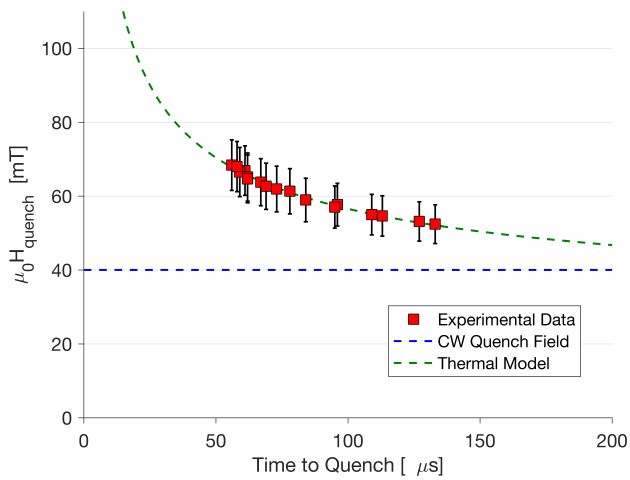

Figure 4: Pulsed quench field as a function of time to reach quench for cavity LTE1-3. This behavior is consistent with a thermal model for a defect limitation, much like cavity LTE1-2.

Nitrogen doped cavities show lower average quench field in general than undoped cavities, with a wide variation in quench field [4]. The pulsed measurements here show that these early quenches are caused by defects and not by a global, fundamental limit; the current model is that doping significantly lowers B_{c1}, thus allowing flux to enter earlier at defect regions with a reduced energy barrier [5]. This serves as evidence that the limits of nitrogen doping may be pushed further. Future work will investigate surface defects and flux entry more deeply in order to determine the next steps in reaching higher quench fields in both CW and pulsed operation.

ISBN 978-3-95450-147-2

Nb_3Sn Cavity

The Nb_3Sn cavity, labeled LTE1-6, exhibited behavior different from the two nitrogen-doped cavities [3]. Figure 5 shows these results. Here, the peak surface magnetic field as a function of temperature shows two distinct regions following the temperature dependence given in Eq. (1), with two different critical fields. In the high temperature region, near T_c = 17 K, the quench field followed a temperature dependence corresponding with a critical field of $B(T = 0)$ = 150 mT. Below 15 K, there is a sharp transition to an even lower critical field, $B(T = 0)$ = 70 mT. This lower field is only slightly higher than the CW quench field of 65 mT.

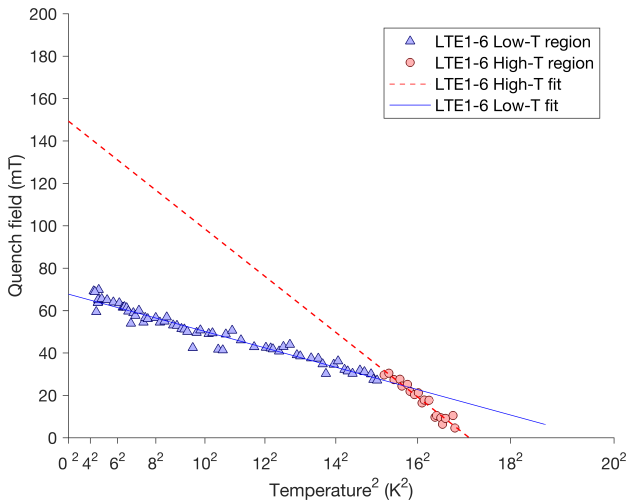

Figure 5: Peak surface magnetic field as a function of temperature for Nb_3Sn cavity LTE1-6, shown here on the scale of $(T/T_c)^2$.

As previously reported in [3], this split between two critical fields seems to indicate multiple Nb_3Sn phases in the cavity, each with different critical fields. This is consistent with surface analysis, which shows regions of low-tin-content Nb_3Sn interspersed among the stoichiometric region which makes up the majority of the Nb_3Sn layer [6]. These tin-depleted regions have a lower critical temperature T_c which can go as low as 6 K, in comparison to the optimal T_c=18 K, and lower even than the critical temperature of niobium, T_c=9 K. These regions may also have lower critical fields. Due to the low thermal conductivity of Nb_3Sn, it is possible that these regions are more susceptible to thermal runaway from flux entry or from normal-conducting losses due to having a lower critical temperature. Future studies will examine these tin-depleted regions to better understand them and reduce their effects.

CONCLUSIONS

We have used a 1 MW 1.3 GHz Klystron to perform high-power pulsed measurements of SRF cavities made from nitrogen-doped niobium and niobium-3-tin. Results for the N-doped cavities are consistent with a thermal model of defect limitation, suggesting that the cavities were limited by either flux entry or thermal heating at a defect. The Nb_3Sn cavity showed results that indicate two separate regions with two distinct limiting critical fields. These may correspond to regions of low and high tin concentration, which have been observed in surface analysis studies. Further work for both these materials will look towards increasing the limiting fields, by limiting the influence of defects in the case of N-doped Nb, and by reducing the presence of tin-depleted regions in Nb_3Sn.

REFERENCES

[1] S. Posen, N. Valles, and M. Liepe. Radio frequency magnetic field limits of nb and nb_3Sn. *Phys. Rev. Lett.*, 115:047001, Jul 2015.

[2] D. L. Hall, T. Gruber, J. J. Kaufman, M. Liepe, J. T. Maniscalco, S. Posen, B. Yu. Nb3Sn Cavities: Material Characterization and Coating Process Optimization. In *Proceedings of SRF 2015*, 2015.

[3] D. L. Hall, H. Conklin, T. Gruber, J. J. Kaufman, M. Liepe, J. T. Maniscalco, T. Proslier, B. Yu. Surface Analysis and Material Property Studies of Nb3Sn on Niobium for Use in SRF Cavities. In *Proceedings of SRF 2015*, 2015.

[4] D. Gonnella, T. Gruber, J. Kaufman, P. Koufalis, M. Liepe, and J.T. Maniscalco. Fundamental Studies on Doped SRF Cavities. In *Proceedings of SRF 2015*, 2015.

[5] D. Gonnella, R. Eichhorn, F. Furuta, M. Ge, T. Gruber, G. Hoffstaetter, J. Kaufman, P. N. Koufalis, M. Liepe, J. T. Maniscalco. Improved N-Doping Protocols for SRF Cavities. In *Proceedings of IPAC 2016*, 2016.

[6] D. L. Hall, J. J. Kaufman, M. Liepe. Surface Analysis Studies of Nb3Sn Thin Films. In *Proceedings of IPAC 2016*, 2016.

ISBN 978-3-95450-147-2